CrossMark click for updates

Mechanisms for plasma cryogenic etching of porous materials

Quan-Zhi Zhang,[1,a)] Stefan Tinck,[1] Jean-François de Marneffe,[2] Liping Zhang,[2] and Annemie Bogaerts[1]
[1]*Research Group PLASMANT, University of Antwerp, Universiteitsplein 1, B-2610 Antwerp-Wilrijk, Belgium*
[2]*IMEC, Leuven 3001, Belgium*

(Received 8 August 2017; accepted 16 October 2017; published online 26 October 2017)

Porous materials are commonly used in microelectronics, as they can meet the demand for continuously shrinking electronic feature dimensions. However, they are facing severe challenges in plasma etching, due to plasma induced damage. In this paper, we present both the plasma characteristics and surface processing during the etching of porous materials. We explain how the damage occurs in the porous material during plasma etching for a wide range of chuck temperatures and the responsible mechanism for plasma damage-free etching at cryogenic temperature, by a combination of experiments and numerical modeling. *Published by AIP Publishing.*
https://doi.org/10.1063/1.4999439

As the electronic feature dimensions in the semiconductor industry are continuously shrinking, porous materials are increasingly being used as inter-metal insulators to address the critical need for a low dielectric constant (low-k).[1–5] However, a lower dielectric constant normally requires an increased pore size and interconnectivity, which will induce a high sensitivity to plasma processing, as radicals and ions can easily penetrate into the interconnected pores, causing severe damage and degrading the dielectric properties.[6–11] Specifically when the feature dimensions drop to 14 nm,[12] the damage depth can be comparable with the narrow trench structures,[13,14] which will result in a significant degradation of the low-k material quality and a non-optimal isolation of adjacent metal lines. Therefore, protection of porous materials becomes crucial during plasma processing.

Among many different protection strategies,[12,15–19] the pore stuffing approaches are the most straightforward and efficient way.[16–19] By filling the pores with a polymer material, the penetration of radicals can be impeded, allowing the protection of the porous material. Compared to traditional pore stuffing approaches with pore stuffing and de-stuffing processes, an alternative protection approach, still in the research phase, was recently proposed,[14] and it also shows high potential for limited plasma induced damage (PID) during plasma etching. By cooling the wafer to cryogenic temperature in fluorocarbon based gas (e.g., C_4F_8 and C_6F_6) before plasma processing, this gas may condense in the pores as liquid, which can prevent the diffusion of radicals into the interconnected pores during the subsequent plasma etching. Finally, after etching, the wafer is brought back to room temperature so that the condensed gas will evaporate, releasing the pores again. Although the concept of cryogenic filling is simple, the underlying mechanisms can be quite complicated, as both the cryogenic temperature and the filling can affect the plasma behavior. All previous research on cryogenic pore filling is solely experimental, which is very valuable but provides limited insights. The inherent mechanisms and the interaction between the plasma and "pore filling" remain indeed very poorly understood.

In this work, we will describe the responsible mechanisms for damage-free cryogenic etching of a porous low-k material, both experimentally and numerically. Our simulations will show how the PID evolves in the inter-connected pores, how the protection occurs in the pores filled with the condensed material, and how the plasma behaves at cryogenic temperature when the pore is filled. The insights obtained from this work are, however, not limited to cryogenic etching, and they might apply to other stuffing protection strategies for porous materials as well.

To experimentally examine the protection effect of the porous material in condensation-based cryogenic etching, a porous organosilicate low-k dielectric material, indicated as p-SiOCH, with an open porosity of 46% and a pore radius of 1.7 nm is being etched by an inductively coupled plasma (ICP) in a mixture of C_4F_8 and SF_6. The etching is conducted at different chuck temperatures, and all the samples are dipped into 0.5% diluted hydrofluoric (dHF) acid liquid for 30 s after etching. Dipping in dHF is used to evaluate the degree of PID, as the bonds of the terminal Si-CH_3 group in p-SiOCH can protect the low-k matrix from dHF, but the PID will remove the CH_3 groups from the pores of p-SiOCH, which makes the porous material chemically reactive with dHF.[20] Therefore, after dipping into dHF acid, cross-sectional inspection will point out which part of the material is damaged by plasma species and removed by dHF.

Figure 1 shows a cross-section of the obtained etching profiles, measured by scanning electron microscopy (SEM). At $-50\,^{\circ}$C, both the trench bottom and the sidewalls are roughly etched (top left corner), as the F-containing radicals from the plasma penetrate into the pores and react with the internal material. Furthermore, the trench sidewalls (patterned structure) are completely removed after dipping in dHF (top right corner). This indicates that significant chemical reactions occurred throughout the sidewalls separating two trenches, i.e., the sidewall damage depth exceeds the spacing width. In contrast, the surface roughness after plasma etching is much improved, and all the trench sidewalls are

[a)]Author to whom correspondence should be addressed: Quan-Zhi.Zhang@uantwerpen.be

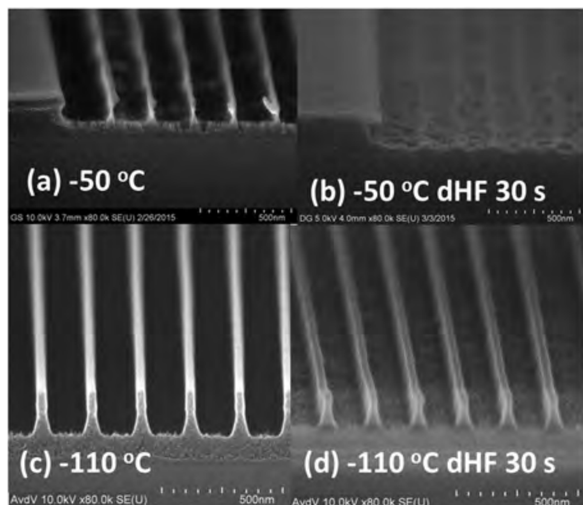

FIG. 1. Cross-sectional images of narrow spacing trench profiles (30 nm low-k line at a pitch of 180 nm) by SEM after plasma etching (left) and 0.5% dHF dip (right), at −50 °C (top) and −110 °C (bottom).

preserved under the protection of condensed C_4F_8 gas at −110 °C (see the bottom left and right corner of Fig. 1).

To examine what is exactly happening inside the pores during etching, we study the etching mechanisms of two adjacent narrow trenches, made of a porous SiO_2 dielectric material, by means of a 2D Monte Carlo model, which forms part of a hybrid plasma model.[21,22] More details about this model, as well as the chemistry included in the model (i.e., list of species and reactions in the gas phase and at the surface), can be found in the supplementary material.

We study the etching mechanisms for different filling degrees of the porous material. We calculate the filling percentage of the pores based on the variation of the refractive index measured from experiments, as in Ref. 14. Furthermore, based on the measured dependence of the refractive index on chuck temperature in Ref. 16, we can estimate the filling percentage at different chuck temperatures (see the detailed explanation in the supplementary material).

In our model, we consider 3 different scenarios, i.e., no filling (or 100% porous) at −50 °C, 15% filling at −104 °C, and 50% filling at −110 °C. Although the pores are completely interconnected in three-dimensional space in the case of no filling, it is not possible to have a 100% connected porous network in a 2D model, as the pores need to be randomly located in the cross-section of the material. We thus consider a somewhat larger porosity of 60% (instead of 46% in the experiments) to account for the larger interconnectivity, when comparing with the experimental data. The average pore radius is also 1.7 nm, like in the experiments. The condensed C_4F_8 uniformly fills up the pores from the edges to the centre at an increasing filling degree. A calculated self-bias of −115 V develops on the RF electrode, which corresponds to the experimental self-bias of −120 V.

Figure 2 shows the calculated etch profiles at different chuck temperatures (corresponding to the different pore filling percentages mentioned above), for a fixed etch time of 160 s. The red color, most clearly observed in Fig. 2(a), indicates the permeation of plasma species and their reactions with the pores, leading to PID. The interconnected porous network acts as a channel for the penetration of F-containing radicals, causing severe damage to the material stucture. This can be observed more clearly from the etching movies in the supplementary material of this paper. Specifically, the middle trench sidewall becomes damaged from two sides at the same time. In the end, it will become severely damaged and the main part of the middle trench will be removed by dHF, which corresponds to the experimental results in Figs. 1(a) and 1(b). Indeed, in practice, more channels will be created as the damage develops, finally crossing each other, so that the radicals can diffuse deeper and deeper.

When lowering the temperature to −104 °C (corresponding to 15% pore filling), the two etched trenches become absolutely independent and the penetration of radicals in the sidewalls is significantly impeded; see Fig. 2(b). At −110 °C (50% pore filling), there are almost no penetration channels anymore [see Fig. 2(c)], the porous material starts to become well protected, as most pores will be separated from each other, and the penetration channels cannot be developed. The etching profile corresponds to the experimental results in Figs. 1(c) and 1(d). When further lowering the temperature to −115 °C and −120 °C, the porous material can be almost perfectly protected (see supplementary material for etch profiles at −95 °C, −115 °C, and −120 °C). Hence, upon lowering the chuck temperature (and thus rising the pore filling degree), the material can gradually be protected, but on the other hand, the etch rate also decreases, which can be deduced from the decreased etch depths with lowering chuck temperature for the same etch time in Fig. 2.

To quantitatively evaluate the extent of damage at different chuck temperatures (and thus pore filling degrees), we plot the average damage depth, or the so-called equivalent damage layer (EDL), as a function of chuck temperature in Fig. 3(a), as obtained from the experiments and simulations. The same trend can be observed for both the experiments

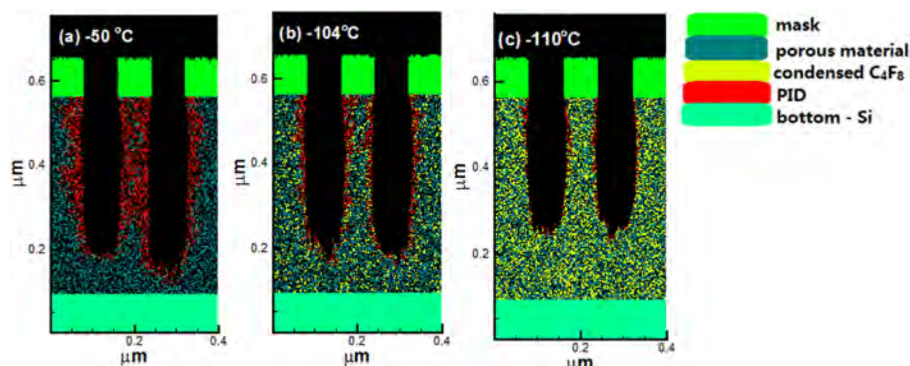

FIG. 2. Calculated trench profiles after plasma etching for 160 s, at (a) −50 °C (no pore filling), (b) −104 °C (15% filling), and (c) −110 °C (50% filling). Multimedia views: https://doi.org/10.1063/1.4999439.1; https://doi.org/10.1063/1.4999439.2; https://doi.org/10.1063/1.4999439.3

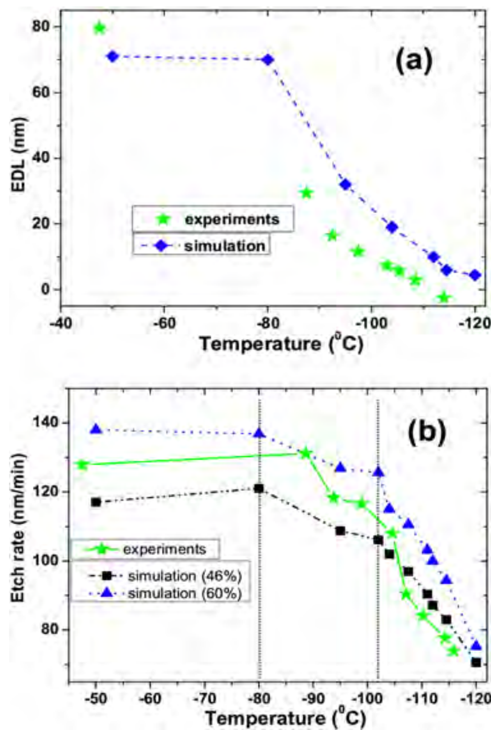

FIG. 3. (a) Equivalent damage layer (EDL) obtained from the experiments using Fourier Transform Infrared Spectroscopy and from the simulations by averaging the damage depth along the trench sidewall; (b) experimental etch rate at a porosity of 46% (derived from Ref. 14) and obtained from the simulations at porosities of 46% and 60%.

and the simulations. The EDL decreases monotonously upon lowering the chuck temperature below −80 °C (i.e., the temperature at which C_4F_8 starts to condense[14]) because C_4F_8 condenses inside the pores, which significantly reduces the number of penetration channels between the pores. The EDL values from both experiments and simulations become extremely small when the temperature approaches −110 °C.

The condensed C_4F_8 is mainly removed by ion bombardment, which explains why the etching takes place in the vertical direction and not in the horizontal direction, as the ions are accelerated by the electric field, arriving at the wafer in the perpendicular direction, and thus, they mainly bombard the trench bottom and not the sidewalls. In Fig. 3(b), the etch rate is plotted as a function of chuck temperature, as obtained from the experiments at a porosity of 46%, as well as from the simulations at both porosities of 46% and 60%. A good qualitative agreement is achieved between the experimental and simulation results.

The variation in the etch rate upon decreasing the chuck temperature can be generally divided into 3 segments, as shown in Fig. 3(b): from −50 °C to −80 °C, from −80 °C to −102 °C, and from −102 °C to −120 °C. Between −50 °C and −80 °C, the etch rate is nearly constant, as there is virtually no filling inside the pores. The slight change in the etch rate is because of the variation in fluxes of the plasma species arriving at the wafer at different chuck temperatures. Between −80 °C and −102 °C, the pores are gradually filled to a certain degree. Since the filling should first be removed by ion sputtering before etching can take place, the etch rate is thus reduced. However, the filling degree is still quite small (<15%) within this temperature range, and so, the reduced connectivity between the pores can still be quite easily repaired and the total etch rate decreases only moderately. Between −102 °C and −120 °C, the degree of filling increases from 15% to 100%, and the more significant drop in the etch rate upon lowering the chuck temperature is largely attributed to the more difficult removal of the filling inside the pores. Meanwhile, the variation of plasma characteristics (see below) also affects the etch rate to a certain degree.

To better understand the responsible mechanisms and plasma behavior in cryogenic etching, we further examine the distributions of plasma species (F and C_2F_4) and ion energy bombarding of the wafer at −50 °C and −120 °C in Fig. 4.

Both F and C_2F_4 reach a maximum density near the coil at both temperatures of −50 °C and −120 °C. This is because of the strongest electromagnetic field at this position, and consequently, most ionization and dissociation reactions take place here. However, the gas number density becomes higher at lower gas temperature (following the ideal gas law), which can induce a higher collision frequency, and therefore, a somewhat higher F and C_2F_4 density appears above the bottom electrode at −120 °C (see yellow color). Since the C_2F_4 molecules have a much higher mass than the F atoms, they will not be so much affected by diffusion, and therefore, the increase in the C_2F_4 concentration above the bottom electrode is a bit more pronounced. This induces a 17% increase for the F flux vs. 32% increase for the C_2F_4 flux to the wafer at −120 °C. Although F is the main reactive etching species, C_2F_4 contributes to the passivation layer on the material and the etching only occurs after removing this passivation layer by reactions with F atoms and ion sputtering.[22] Therefore, the relatively high increase in C_2F_4 flux with lower temperature may also reduce the etch rate. Furthermore, the higher concentration of all neutrals enhances the collision frequency between the species above the wafer at low temperature, which induces a smaller self-bias. Indeed, the self-bias is always lower in a collisional plasma than in a collisionless plasma.[23] Consequently, there is a drop of almost 20 eV in the ion energy. This also contributes a bit to the lower etch rate.

In conclusion, we have explored the evolution of plasma damage inside a porous material as a function of chuck temperature and the responsible protection mechanism by cryogenic etching. The results of the numerical model are in very good agreement with the experimental data, and so, the model allows us to provide insight into the protection strategy of porous material processing. The interconnected porous network acts as a penetration channel for the radicals, which causes deep damage into the material stucture, and it can even destroy the dielectric spacing, leading to structure loss. When lowering the chuck temperature, the C_4F_8 gas used for pore stuffing gradually condenses inside the porous material and fills the pores. This pore filling can mitigate the PID at the sidewalls and also reduce the connectivity between the pores, i.e., the penetration channels of the radicals, which decreases the damage depth into the material. When the pore filling degree reaches 50%, the porous material starts to become well protected. However, since the filling first needs to be removed by ion sputtering before etching can proceed, the etch rate is also significantly reduced upon lowering the chuck temperature. Therefore, a chuck temperature of around

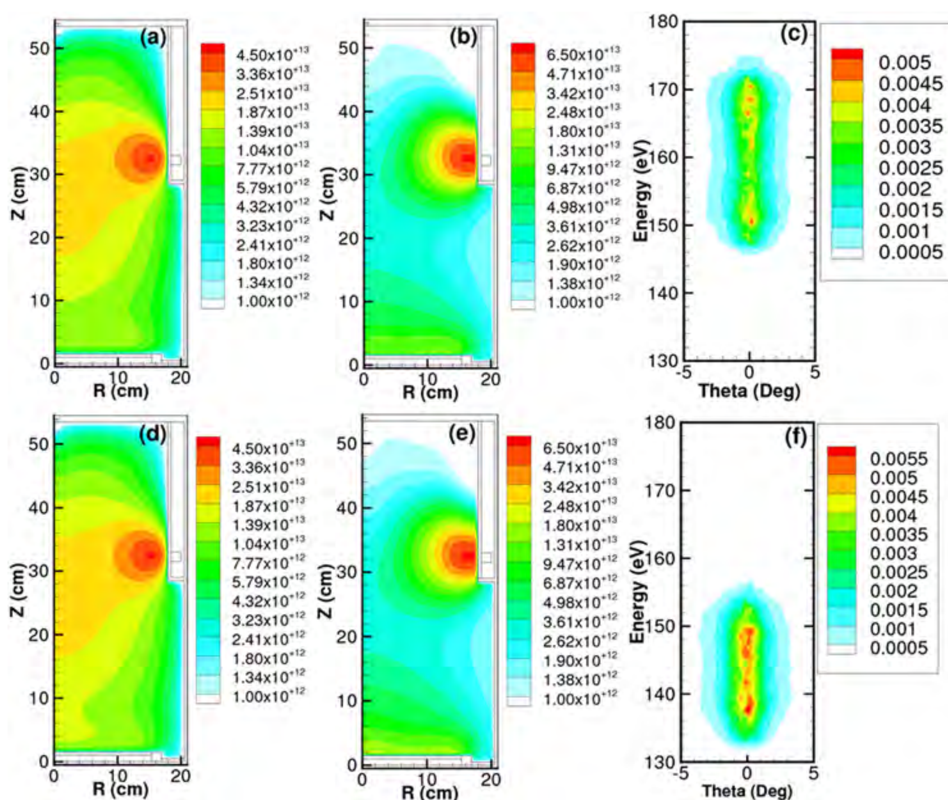

FIG. 4. Calculated (a) and (d) F atom density (in cm^{-3}), (b) and (e) C_2F_4 molecule density (in cm^{-3}), and (c) and (f) normalized ion energy and angular distributions, at $-50\,^{\circ}C$ (a)–(c) and $-120\,^{\circ}C$ (d)–(f).

$-104\,^{\circ}C$ might be more beneficial, as it yields limited damage (in spite of the moderate filling degree of 15%), while still allowing significant etching. Meanwhile, the distributions of plasma species and consequently the neutral fluxes and ion energy are affected by the cryogenic temperature, which also lowers the etch rate. These insights into the plasma behavior and the etch evolution help us to understand the fundamental mechanisms in cryogenic etching.

See supplementary material for the more experimental and model details.

We acknowledge the support from Marie Skłodowska-Curie actions (Grant Agreement-702604). This work was carried out in part using the Turing HPC infrastructure at the CalcUA core facility of Universiteit Antwerpen, a division of the Flemish Supercomputer Center VSC, funded by the Hercules Foundation, the Flemish Government (department EWI), and the University of Antwerp. L. Zhang and J.-F. de Marneffe acknowledge Dr. M. Cooke and A. Goodyear from Oxford Instruments Plasma Technology for processing the samples at their Yatton facility in the United Kingdom.

[1]J. L. Hedrick, R. D. Miller, C. J. Hawker, K. R. Carter, W. Volksen, D. Y. Yoon, and M. Trollsås, Adv. Mater. **10**, 1049 (1998).
[2]R. D. Miller, Science **286**, 421 (1999).
[3]S. J. Martin, J. P. Godschalx, M. E. Mills, E. O. Shaffer, and P. H. Townsend, Adv. Mater. **12**, 1769 (2000).
[4]M. Baklanov, M. Green, and K. Maex, *Dielectric Films for Advanced Microelectronics* (Wiley, New York, USA, 2007).
[5]W. Volksen, R. D. Miller, and G. Dubois, Chem. Rev. **110**, 56 (2010).
[6]Y. Furukawa, M. Patz, T. Kokubo, and J. H. M. Snijders, Microelectron. Eng. **70**, 267 (2003).
[7]S. L. Xu, C. Qin, L. Diao, D. Gilbert, L. Hou, and A. Wiesnoski, J. Vac. Sci. Technol., B **25**, 156 (2007).
[8]A. Franquet, M. Claes, T. Conar, E. Kesters, G. Vereecke, and W. Vandervorst, Appl. Surf. Sci. **255**, 1408 (2008).
[9]Y. Iba, T. Kirimura, M. Sasaki, Y. Kobayashi, Y. Nakata, and M. Nakaishi, Jpn. J. Appl. Phys., Part 1 **47**, 6923 (2008).
[10]K. Takeda, Y. Miyawaki, S. Takashima, M. Fukasawa, K. Oshima, K. Nagahata, T. Tatsumi, and M. Hori, J. Appl. Phys. **109**, 033303 (2011).
[11]M. Darnon and T. Chevolleau, J. Vac. Sci. Technol., B **31**, 061206 (2013).
[12]N. Inoue, paper presented at the IEEE International Electron Devices Meeting, Washington, USA, December 2013.
[13]Q. T. Le, M. R. Baklanov, E. Kesters, A. Azioune, H. Struyf, W. Boullart, J.-J. Pireaus, and S. Vanhaelemeersch, Electrochem. Solid-State Lett. **8**, F21 (2005).
[14]L. P. Zhang, J.-F. Marneffe, F. Leroy, P. Lefaucheux, T. Tillocher, R. Dussart, K. Maekawa, K. Yatsuda, C. Dussarrat, A. Goodyear, M. Cooke, S. D. Gendt, and M. R. Baklanov, J. Phys. D: Appl. Phys. **49**, 175203 (2016).
[15]O. V. Braginsky, A. S. Kovalev, D. V. Lopaev, E. M. Malykhin, Y. A. Mankelevich, T. V. Rakhimova, A. T. Rakhimov, A. N. Vasilieva, S. M. Zyryanov, and M. R. Baklanov, J. Appl. Phys. **108**, 073303 (2010).
[16]T. Frot, W. Volksen, S. Purushothaman, S. Bruce, and G. Dubois, Adv. Mater. **23**, 2828 (2011).
[17]T. Frot, W. Volksen, S. Purushothaman, R. S. Bruce, T. Magbitang, D. C. Miller, V. R. Deline, and G. Dubois, Adv. Funct. Mater. **22**, 3043 (2012).
[18]M. Heyne, L. Zhang, J. Liu, I. Ahmad, D. Toma, J.-F. Marneffe, S. Gendt, and M. R. Baklanov, J. Vac. Sci. Technol., B **32**, 062202 (2014).
[19]K. Lionti, W. Volksen, T. Magbitang, M. Darnon, and G. Dubois, ECS J. Solid State Sci. Technol. **4**, N3071–N3083 (2015).
[20]M. R. Baklanov, J. F. Marneffe, D. Shamiryan, A. M. Urbanowicz, H. L. Shi, T. V. Rakhimova, H. Huang, and P. S. Ho, J. Appl. Phys. **113**, 041101 (2013).
[21]M. Kushner, J. Phys. D: Appl. Phys. **42**, 194013 (2009).
[22]A. Sankaran and M. Kushner, J. Vac. Sci. Technol., A **22**, 1242 (2004).
[23]Q. Z. Zhang, W. Jiang, L. J. Hou, and Y. N. Wang, J. Appl. Phys. **109**, 013308 (2011).